slope of the resulting straight line is 2.0, remarkably close to the value of the Grüneisen constant Γ for Cu (1.96). This value can be calculated directly from the expression $-\partial \ln \Theta_D / \partial \ln V = 3V\delta / kc_V \equiv \Gamma$, where δ is the linear expansion coefficient, k is the compressibility, c_v is the specific heat, and V is the volume. While the above expression is only an approximation, it describes surprisingly accurately the behvaior of experimental results. Our measurements of the Debye-temperature trend on alloying with Sn yields $d\ln\Theta_D/d\vartheta = -0.48 \pm 0.02$. This value lies closer to the straight line on Fig. 6, thus further improving the agreement between the value of the Grüneisen constant Γ and the slope of the line as determined from other experimental results. We conclude that in Cu-based alloys the rate of change of the Debye temperature when normalized in terms of ϑ, depends mostly on size effects. Other contributions, such as, for example, electron-phonon interaction, appear to be less dependent on the particular solute and its valence, and more on the value of the electron concentration.

ACKNOWLEDGMENTS

The authors wish to acknowledge the assistance of Jan Kajuch in the experimental work and George Dadok for skillful assistance in the computer analysis.

[1]See, e.g., A. H. Wilson, *The Theory of Metals*, 2nd ed. (Cambridge U. P., Cambridge, England, 1953).
[2]H. Jones, Proc. Roy. Soc. (London) A49, 250 (1937).
[3]J. S. Faulkner, H. L. Davis, and H. W. Joy, Phys. Rev. 161, 656 (1967).
[4]M. M. Cohen and V. Heine, Advan. Phys. 7, 395 (1958).
[5]H. Jones, Proc. Roy. Soc. (London) A240, 321 (1957).
[6]E. A. Stern, Phys. Rev B 1, 1518 (1970).
[7]P. Soven, Phys. Rev. 151, 539 (1966).
[8]H. Amar, K. H. Johnson, and C. B. Sommers, Phys. Rev. 153, 655 (1967).
[9]L. C. Clune and B. A. Green, Jr., Phys. Rev. 144, 525 (1966).
[10]J. Bevk, V. Sein, and S. Noguchi (unpublished).
[11]U. Mizutani, S. Noguchi, and T. B. Massalski, Phys. Rev. B 5, 2057 (1972).
[12]J. R. Frank, F. D. Manchester, and D. L. Martin, Proc. Roy. Soc. (London) A263, 494 (1961).
[13]A. Will and B. A. Green, Phys. Rev. 150, 519 (1966).
[14]J. K. Lees and P. A. Flinn, Phys. Rev. B 3, 591 (1970).
[15]H. C. Yeh and L. V. Azaroff, J. Appl. Phys. 38, 4034 (1967).
[16]K. Fujiwara, O. Sueoka, and T. Imura, J. Phys. Soc. Japan 24, 467 (1968).

PHYSICAL REVIEW B VOLUME 5, NUMBER 12 15 JUNE 1972

Fermi Surface of Lead at Normal and High Pressure*

J. R. Anderson
Department of Physics and Astronomy, University of Maryland, College Park, Maryland 20742
and
W. J. O'Sullivan† and J. E. Schirber
Sandia Laboratories, Albuquerque, New Mexico 07115
(Received 3 November 1971)

The pressure dependence of the Fermi surface of lead has been studied by means of NMR-calibrated de Haas—van Alphen—effect measurements. In order to carry out these investigations, the values of Fermi-surface areas, obtained from pulsed-magnetic-field measurements, have been redetermined to correct for a calibration error. Attempts to fit the measurements with a local model potential were not completely successful, but a nonlocal calculation based on the Heine-Abarenkov model potential gave satisfactory agreement with the experimental results.

I. INTRODUCTION

There has been considerable interest recently in the Fermi surface of lead and in pseudopotential models used to describe this surface. This is partly due to the fact that lead is a strong-coupling superconductor whose density of states has been determined from electronic-tunneling[1] and specific-heat[2] measurements. In addition there is a great wealth of experimental information about the electronic structure of lead, e.g., de Haas–van Alphen (dHvA) effect,[3] cyclotron resonance,[4,5] magneto-acoustic[6] effect, optical properties,[7,8] and Kohn effect.[9]

A calibration error was discovered in previous pulsed-field experiments[3] (hereafter referred to as I) making it desirable to remeasure the dHvA frequencies for magnetic field H along symmetry di-

rections. These measurements have been made using *in situ* NMR[10] for $H \parallel [100]$, [110], and [111]. Along with these dHvA experiments at normal pressure, measurements were made at higher pressures to study the effect of lattice spacing changes on the Fermi surface. These pressures studies are a more complete investigation of work reported earlier.[11]

In a previous report[3] the Fermi surface of lead was described by means of a parametrized, local, pseudopotential model with four parameters including the Fermi energy. It has not been possible to adequately describe the pressure dependence of the Fermi surface with this model, and consequently a simple nonlocal model based on the Heine-Abarenkov model potential has been used to fit the experimental results.

In Sec. II the experimental approach is described, in Sec. III the Fermi surface is discussed in terms of the empty-lattice model, while in Sec. IV the experimental results are given. In Sec. V the nonlocal calculation is discussed and the calculated results are compared with experiment in Secs. VI and VII.

II. EXPERIMENTAL PROCEDURE

de Haas–van Alphen frequencies have been measured for the magnetic field H along the symmetry directions using a 55-kG superconducting magnet with homogeneity about 3 parts in 10^5 over a $\frac{1}{2}$-in. diameter sphere. In general, the magnetic field was determined with the Al^{27} NMR resonance corrected for the Knight shift (1.1112 MHz/kOe).

The low-frequency field-modulation technique[12] was used, with the dHvA signal picked up by a compensated pickup coil. The modulation frequency was typically between 40 and 100 Hz. This fundamental frequency was filtered from the output of the pickup coil and the remaining harmonics, after amplification, became the input to a lock-in amplifier. In these experiments it was especially important to pick out only one particular dHvA component for study which was done with the Bessel-function selection technique.[13] That is, the amplitude of the nth harmonic of the modulation frequency is proportional to a Bessel function $J_n(\alpha)$, where $\alpha = 2\pi F h_m / H^2$; F is the dHvA frequency, h_m is the modulation field amplitude, and H is the large dc magnetic field. A particular choice of h_m (kept proportional to H^2) allowed rejection of unwanted dHvA frequencies. In this way, by carefully choosing n and h_m, it was possible to separate one de Haas–van Alphen frequency from another that differed by only a few percent. With measurement of several hundred cycles, as was usually possible with this approach, the error in dHvA frequency is thought to be less than 0.1% for most of the results reported here.

Two approaches used in the pressure studies were (i) high-pressure solid-helium technique,[14] and (ii) fluid-helium phase-shift technique.[15] For the solid-helium measurements, pressures up to 4 kbar were used while only about 25 bar were possible for the fluid-helium studies at about 1.2 °K. Both techniques have been well described in the literature and will not be discussed in detail here. The fluid-helium approach is simpler and quicker, and, if the pressure dependence is linear, the phase-shift results are all that are needed. In lead, both methods were used for several sets of oscillations and the agreement was good. This is not always the case; for example, in antimony the sign of the derivative of the dHvA frequency with pressure actually reverses at high pressures.[16]

III. FERMI-SURFACE DESCRIPTION

The Fermi surface of lead has been shown to agree qualitatively with the empty-lattice model for a face-centered-cubic structure with four valence electrons per atom.[3,17] The low-temperature lattice constant a has been estimated from thermal expansion data to be about 4.90 Å.[3] The contributions to the Fermi surface belong to the second and third zones and have been shown schematically in I. The second zone is a large centrosymmetric surface containing holes, while the third zone consists of a multiply connected surface of {110}-direction arms. The relevant extremal orbits and nomenclature are also shown in I and will now be described briefly.

(i) ψ. This orbit is a large orbit on the second-zone hole surface with center at the Brillouin-zone center Γ. There are no noncentral orbits expected for this surface because of the rather large rounding by the potential.

(ii) ζ. This is an orbit around a third-zone-arm cross section centered at the symmetry point K (or U). The minimum cross section is in a (110) plane.

(iii) ν. This is an orbit about the junction of four arms and is centered at the point W. There is a minimum area in a (100) plane. This surface is somewhat complicated as shown by the presence of beats in the dHvA oscillations about 600 cycles long[18,19] for the magnetic field along [100]. (Analysis shows that the beats are produced because there is a second extremal section near W with area about 0.17% larger). For $H \parallel [110]$, dHvA oscillations would also be expected to result from this surface, orbit ω, but searches for their existence are somewhat inconclusive, as the estimated frequency resulting from such a section is very nearly that of the second harmonic of orbit ζ.

(iv) ξ. This is an orbit on the inside of a square face centered at X and has a minimum area in a (100) plane.

TABLE I. dHvA frequencies and their pressure derivatives.

		F (MG)			$\frac{d\ln F}{dP}$ (10^{-3} kbar^{-1})				
			Calculated[a]			local		Calculated nonlocal	
Orbit	Direction	Experimental	local	nonlocal	Experimental	R_M constant	R_M scaled	R_M constant	R_M scaled
ν[b]	[100]	51.25 ± 0.01[b]	51.43	51.22	2.3 ± 0.1[c] 2.7 ± 0.4[d]	1.5	2.1	1.6	2.5
ζ[b]	[110]	18.09 ± 0.02[e]	18.24	18.14	2.5 ± 0.2[c] 2.4 ± 0.6[d]	1.4	2.2	2.1	2.8
ζ[b]	[111]	22.37 ± 0.0	22.76	22.50	2.7 ± 0.2[c]	1.4	2.2	2.1	2.8
ω	[110]		39.35	39.24		1.6	2.6		
θ[b]	[111]	109.5 ± 0.3	110.0	109.3	1.2 ± 0.1[c]	1.1	0.4	1.4	1.0
ξ	[100]	36.04 ± 0.2	33.85	34.83	0.0 ± 0.3[c]	2.0	2.7	0.0	−0.1
ψ[b]	[110]	159.11 ± 0.05	161.28	159.21	2.9 ± 0.2[c] 3.1 ± 0.4[d]	1.3	1.5	1.4	2.5
ψ	[111]	155.8 ± 0.4	153.4	153.6	2.1 ± 0.2[c]	1.4	1.6	1.3	2.1
ψ	[100]	204.4 ± 0.4	208.1	201.7	2.4 ± 0.4[c]	1.3	1.6	1.5	2.4
dev.[f]			0.013	0.008					

[a]dHvA frequency in gauss has been determined by multiplying the cross-sectional area, in units of $(2\pi/a)^2$, by 1.724×10^8.

[b]Used in the least-squares fit for the nonlocal model.

[c]Fluid He.

[d]Solid He to ≈ 4 kbar.

[e]At this orientation there is some ambiguity because of another frequency about 2.4% lower. It has been assumed here that this second frequency results from a noncentral cross section of a third-zone arm.

[f]rms fractional deviation with orbit ξ omitted.

(v) θ. This is an orbit on the inside of a hexagonal face centered at L and has a minimum area in a (111) plane.

IV. dHvA MEASUREMENTS

Accurate dHvA-frequency measurements have been made corresponding to the above orbits, and the results are shown in Table I. Since the fields were measured to at least 0.05% with *in situ* NMR, the uncertainty in the frequencies is generally of the order of 0.1%. (Larger errors are found for the weaker oscillations, e.g., ξ[100], and for oscillations with frequencies which vary rapidly with orientation, e.g., ζ[111].) Thus these measurements provide a rather stringent test of any Fermi-surface model.

The pressure derivatives $d\ln F/dP$ are also shown in Table I. For three of the sets of oscillations, both phase-shift and high-pressure studies were made and the agreement was well within the experimental error. For a cubic system, the simplest model prediction for the change with pressure of the Fermi surface is that of free-electron scaling; the basic assumption of this model is that the same fraction of the Brillouin zone remains filled when the lattice spacing is changed. Scaling thus requires that all cross sections increase at the rate of $\frac{2}{3}$ the value of the compressibility. The compressibility of lead, K_T, at 4 °K is about 2.05×10^{-3}/kbar,[20] and it should be noted that the changes for both electrons and holes are generally about 2 times the compressibility scaling prediction.

V. FERMI-SURFACE MODELS

As noted above, although the free-electron or empty-lattice model accounts for the general topology of the Fermi surface of lead, it fails seriously when the pressure data are considered. Since lead is a compensated metal, the hole and electron volumes are equal, and both must change in the same way with hydrostatic pressure. Thus it is not surprising that the change is large for both hole and electron sheets as shown for example by orbits ψ and ζ in Table I.

We have calculated cross-sectional areas and pressure derivatives using the parametrized model described in I with form factors obtained from a Heine-Abarenkov *local* model potential.[21,22] The parameters E_F, V_{111}, V_{200}, and λ were determined by a least-squares fit to the experimental dHvA values, where E_F is the Fermi energy, V_{111} and V_{200} are Fourier coefficients of the pseudopotential, and λ is the spin-orbit parameter.[3] Although the resulting cross sections agree fairly well with experiment, the fourth zone is not empty, a problem which will be referred to later. In addition, the calculated pressure derivatives for the hole-surface cross-sectional areas are too small, and there is a particularly large discrepancy between the calculated and observed pressure derivatives for the cross section associated with the ξ orbit.

Thus we have adopted a simple nonlocal model with the form of the lattice and spin-orbit potentials as given by the Heine-Abarenkov-Animalu model potential.[23,24] Instead of using the form factors V_K,

as was done in I and in the local calculation referred to above, in this nonlocal model the ion-core potentials have been replaced by square wells whose depths A_l are treated as adjustable parameters. (The subscript l refers to the angular momentum state projected out of the lattice potential.) Three well depths A_0, A_1, and A_2 have been used with the original Heine-Abarenkov prescription, $A_l = A_2$ for $l > 2$. Although one additional parameter is introduced by this scheme, the results are insensitive to A_2, and only two important parameters describe the lattice potential. The radius of the square well R_M has not been used as a parameter but has either been held fixed at the value used by Animalu and Heine[23] ($R_M = 2.1$ a.u.) or has been allowed to scale with the linear compressibility from the Animalu-Heine value. Since the resulting form factors V_{111} and V_{200}, calculated for given values of A_l, are found to vary appreciably with position in the Brillouin zone, the calculation is nonlocal. For the sake of completeness and in order to describe the nonlocal form of the potential that we have used, the Animalu-Heine[23] model-potential formalism is described briefly below.

Within a "core" region each atomic potential is replaced by a superposition of l-dependent square wells whose dimensions are determined from atomic spectra. The resulting potential is given by

$$V_M(r) = -\sum B_K^l Q_K^l, \quad r < R_M$$
$$= -z/r, \quad r > R_M . \tag{1}$$

The operators Q_K^l project out the l, Kth components from the wave function which consists of the product of a spatially dependent function and a spinor. The K's are related to the spatial angular momentum l and the total angular momentum j by

$$K = l \quad \text{for } j = l - \tfrac{1}{2}$$
$$= -l - 1 \quad \text{for } j = l + \tfrac{1}{2} . \tag{2}$$

We note that

$$A_l = \frac{lB_l + (l+1)B_{-l-1}}{2l+1} \tag{3}$$

is the ordinary-lattice square-well depth, while

$$\lambda_l = (B_l - B_{-l-1}) \frac{2}{2l+1} \tag{4}$$

is the spin-orbit-coupling parameter used here.[24]

In order to apply these results to the lead problem, initial estimates of the square-well depths are obtained by finding the values corresponding to the spectral levels given in Moore's tables[25] for the Pb^{+4} ion and extrapolating to the energy corresponding to the Fermi energy ϵ_F ($\epsilon_F = -2.746$ Ry relative to the ion). Results for $R_M = 2.1$ a.u. are shown in Fig. 1. The A_2-vs-E curve must be extrapolated extensively to reach the Fermi energy, and consequently the extrapolation procedure does not lead to an accurate value for this parameter. In addition, since there is only one atomic p level ($6p$), the value of A_1 is not actually determined at all. The initial square-well values as given by Animalu and Heine[23] and recalculated here are given in Table II along with the final values determined from our nonlocal fitting procedure. It can be seen that the differences are well within the uncertainties of the method. See also Fig. 1, where our final values of $A_l(\epsilon_F)$ are indicated.

The form of the model potential is shown in Fig. 2 for the $l = 0$ states. There is a constant potential

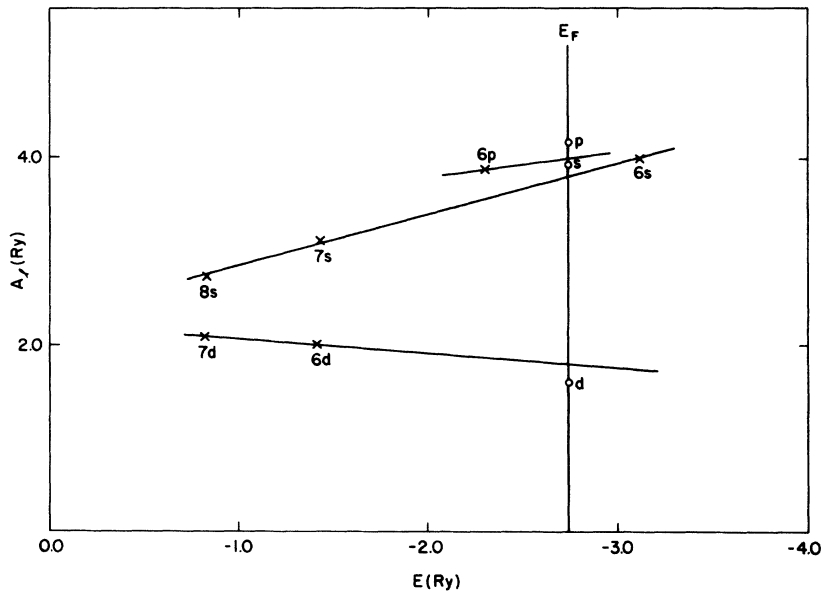

FIG. 1. Determination of square-well depths from spectral energy levels of Pb^{+4} for $R_M = 2.1$ a.u. A straight line has been drawn through the atomic spectral values for each l value, and the intersection with the Fermi energy ϵ_F gives the starting value of A_l. Final values from the least-squares fit are shown by ○.

TABLE II. Parameter values (Ry).

Parameter	Initial value[a]	Final value nonlocal	local
A_0	3.84	3.93[b]	4.00
A_1	4.00	4.2[b]	4.16
A_2	1.8	1.6[b]	1.8
λ_1	0.34	0.55[b]	0.0855 ($\xi_p = 0.066$)[c,d]
E_F	0.709	0.712[b]	0.724[c]
V_{111}	−0.081	−0.070[e]	−0.094[c]
V_{200}	−0.034	−0.019[e]	−0.057[c]

[a]Obtained from atomic-spectral-term values.

[b]Parameters used in nonlocal calculation.

[c]Parameters used in local calculation.

[d]This parameter has a different form from that used in the nonlocal calculation (see I).

[e]Form factors evaluated at the symmetry point W which does not lie on the Fermi surface.

of $-A_0$ for $r < R_M$ and outside this radius a $-z/r$ dependence. The potential is discontinuous at $r = R_M$ which is a disadvantage of the model. It would probably be better to use the approach suggested by Shaw and Harrison[26] in which R_M is adjusted for each l so that there is no discontinuity in the potential. However, this complicates the fitting procedure by requiring calculations of A_l for a number of R_M and also by introducing integrals of Bessel functions, that must be done numerically, into the calculation of form factors. Therefore, in the interests of simplicity we have followed the original approach of Heine and Abarenkov.[21,22]

Once the A_l are obtained, the lattice-potential form factors $V_{\vec{k}\vec{k}'}$ can be determined from

$$V_{\vec{k}\vec{k}'} = (\langle \vec{k} | V_M | \vec{k}' \rangle + V_{cc} + V_{ex} + V_o)/\epsilon(\vec{K}) \ . \tag{5}$$

Here $\vec{K} = \vec{k} - \vec{k}'$, where $\vec{k}$ and $\vec{k}'$ are the initial- and final-state wave vectors. The Hartree dielectric function $\epsilon(\vec{K})$ screens the potential, and V_{cc}, V_{ex}, and V_o are correlation, exchange, and orthogonalization terms, respectively, as given by Animalu and Heine.[23]

The spin-orbit term must be added to the lattice-potential form factors. The resulting spin-orbit matrix elements are also nonlocal, depending upon both initial and final states, and we have calculated these following the approach of Animalu.[24] These matrix elements take the form

$$V^{so}_{\vec{k}\vec{k}'} = i\lambda_1 G_1 \frac{\vec{k}\times\vec{k}'}{|\vec{k}|\,|\vec{k}'|} \cdot \langle \nu' | \vec{\sigma} | \nu \rangle \ , \tag{6}$$

where $\vec{\sigma}$ are the Pauli spin matrices, ν and ν' represent spinors, and

$$G_1 = \frac{6\pi}{\Omega}\int_0^{R_M} j_1(k'r) j_1(kr) r^2 \, dr$$

$$= \frac{6\pi}{\Omega} \frac{R_M^2}{k^2 - k'^2} [k' j_0(k' R_M) j_1(k R_M)$$

$$- k j_0(k R_M) j_1(k' R_M)] \ , \quad k \neq k' \ . \tag{7}$$

We have kept only the p-state splitting λ_1, for simplicity and for ease in comparison with the local model. An initial estimate of λ_1 was made from the atomic spin-orbit splittings[25] of Pb^{+4} and is given in Table II. The spin-orbit parameter used for the local model, which has a different form, is also given in Table II.

The spin-orbit and lattice terms are combined to give the Hamiltonian matrix. As was the procedure in I, we take four orthogonalized plane waves (OPW) combined with spinors, ↑ and ↓, to give eight product wave functions $\psi_1\uparrow$, $\psi_2\uparrow$, $\psi_3\uparrow$, $\psi_4\uparrow$, $\psi_1\downarrow$, $\psi_2\downarrow$, $\psi_3\downarrow$, and $\psi_4\downarrow$. The resultant truncated Hamiltonian, which is complex, is given by

$$\mathcal{H} = \begin{pmatrix} \alpha & \beta \\ -\beta^* & \alpha^* \end{pmatrix} \ , \tag{8}$$

where

$$\alpha = \begin{pmatrix} T_1 & h^I_{12} + X^{so}_{12} & h^I_{13} + X^{so}_{13} & h^I_{14} + X^{so}_{14} \\ h^I_{12} - X^{so}_{12} & T_2 & h^I_{23} + X^{so}_{23} & h^I_{24} + X^{so}_{24} \\ h^I_{13} - X^{so}_{13} & h^I_{23} - X^{so}_{23} & T_3 & h^I_{34} + X^{so}_{34} \\ h^I_{14} - X^{so}_{14} & h^I_{24} - X^{so}_{24} & h^I_{34} - X^{so}_{34} & T_4 \end{pmatrix} . \tag{9}$$

and

$$\beta = \begin{pmatrix} 0 & \psi^{so}_{12} & \psi^{so}_{13} & \psi^{so}_{14} \\ -\psi^{so}_{12} & 0 & \psi^{so}_{23} & \psi^{so}_{24} \\ -\psi^{so}_{13} & -\psi^{so}_{23} & 0 & \psi^{so}_{34} \\ -\psi^{so}_{14} & -\psi^{so}_{24} & -\psi^{so}_{34} & 0 \end{pmatrix} .$$

Here the lattice components are

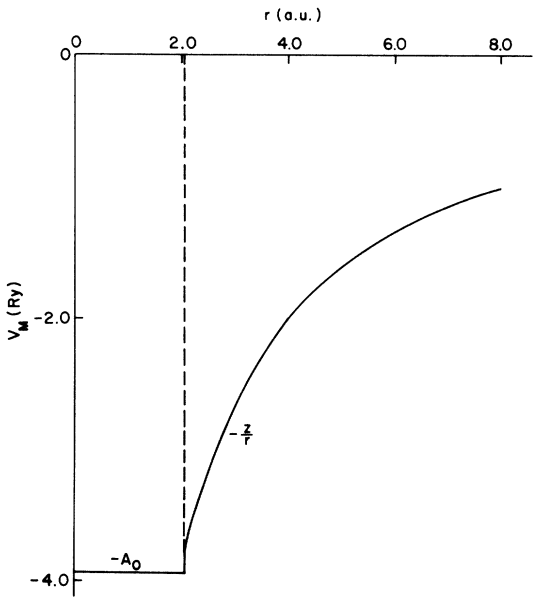

FIG. 2. Model potential for $l = 0$ states.

$$h^{I}_{ij} = V_{\vec{k}_i \vec{k}_j}\ ; \qquad \vec{K} = \vec{k}_i - \vec{k}_j = \begin{cases} [200] \text{ or equivalent directions for } i=1,\ j=2 \text{ and } i=3,\ j=4 \\ [111] \text{ or equivalent directions for } i=1,\ j=3,4 \text{ and } i=2,\ j=3,4\ . \end{cases}$$

The spin-orbit components are

$$X^{so}_{ij} = \langle \vec{k}_i\uparrow \,|\, V_{so} \,|\, \vec{k}_j\uparrow \rangle\ ,$$
$$\psi^{so}_{ij} = \langle \vec{k}_i\uparrow \,|\, V_{so} \,|\, \vec{k}_j\downarrow \rangle\ .$$

In order to avoid working with complex matrices, we double the dimensions of the Hamiltonian matrix to make it real. This can be done by making a 16×16 matrix of the form

$$H = \begin{pmatrix} \mathcal{H} & 0 \\ 0 & \mathcal{H}^* \end{pmatrix}\ ,$$

where $\mathcal{H}$ is the 8×8 Hamiltonian in Eq. (8) and $\mathcal{H}^*$ is the complex conjugate. Then by carrying out the similarity transformation SHS^{-1}, where

$$S = \begin{pmatrix} I & I \\ -iI & iI \end{pmatrix}$$

and I is an 8×8 identity matrix, we obtain the final matrix $H_T = SHS^{-1}$, which is a real, symmetric, 16×16 matrix. Now if the matrix were to be used as it is to develop constant energy surfaces, a complication would arise because each energy level is fourfold degenerate. However, since we wish only to find zeros of the secular determinant resulting from H_T, in order to trace out constant energy surfaces in k space, we can treat this more simply. To this end, the matrix is transformed such that the first four columns refer to the first OPW with spin-up and spin-down paired, while the next four refer to the second, and so on. Then using the Gaussian elimination technique,[27] it is possible to treat four columns or rows at a time.[28] This eliminates the degeneracy complication and serves to speed up the evaluation of the determinant. The latter is important because it may be necessary to compute the value of the determinant more than 1000 times for one orbit on the Fermi surface.

Having determined the A_l's at an energy E_F, we neglect the dependence of A_l upon E in the remainder of the calculation. Of course, it would be possible to determine a Fermi energy, go back and redetermine the A_l's, and so on, but in view of the inaccuracy as shown by Fig. 1, this would not be very meaningful. In fact, the initial guess of Fermi energy was sufficiently close to the final result that this modification was not important.

A least-squares program with the constraint that compensation be maintained was used to give the best fit of five extremal sections (noted in Table I) to experimental dHvA values. This least-squares fit determined the optimum values of the square-well depths, and the energy E_F and the spin-orbit parameter λ_1. These are shown in Table II, and the resulting cross sections are given in the next section.

In the early stages of this work it was supposed that the local component of the model potential would be dominant and that the nonlocal contributions could be included as a small correction. It was quickly discovered, however, that the two types of contribution to the model potential for lead were of roughly equal magnitude and thus we were led to use a description in which the local and nonlocal terms were considered in the same order. The importance of the nonlocal part of our model potential for lead may be inferred from the significant variations in the form factor values as the Fermi surface is traced. In Table III we show values of $V_{kk'}$ averaged around several orbits of the Fermi surface, as one indication of this variation. We see that there are variations among dif-

TABLE III. Form factors averaged for different orbits (Ry).

Orbit	Direction	V_{111}	$V_{1\bar{1}1}$	$V_{11\bar{1}}$	$V_{1\bar{1}\bar{1}}$	V_{200}	$V_{0\bar{2}0}$
ν	[100]	−0.067	−0.080	−0.062	−0.076	−0.023	−0.022
ζ	[110]	−0.069	−0.080	−0.064	−0.076	−0.017	−0.031
ζ	[111]	−0.070	−0.079	−0.064	−0.075	−0.017	−0.028
ω	[110]	−0.078	−0.071	−0.071	−0.065	−0.022	−0.022
θ	[111]	−0.071	−0.062	−0.080	−0.072	−0.023	−0.021
ξ	[001]	−0.072	−0.072	−0.072	−0.072	−0.010	−0.032
ψ	[110]	−0.061	−0.067	−0.083	−0.084	−0.020	−0.041
ψ	[111]	−0.062	−0.063	−0.084	−0.084	−0.021	−0.039
ψ	[010]	−0.065	−0.065	−0.083	−0.083	−0.016	−0.039
Avg.[a]		−0.068	−0.071	−0.073	−0.076	−0.018	−0.030
Δ[b]		25	26	29	26	70	68

[a]Avg. is the average for all nine orbits.

[b]Δ is the maximum variation in percent.

ferent sections of the Fermi surface of the order of 25–30% for the {111} terms and 70% for the {200} terms. We might also note that the second-zone-hole-surface averages are appreciably different from those of the third zone. In Sec. VII we show that this nonlocal model gives much better agreement with the pressure dHvA experiments than the local model. The difficulty with the local model is in explaining the large changes in the second-zone areas with pressure, and the form factor variations noted above (neglected in the local model) may explain the improvement obtained with the nonlocal calculations.

VI. NORMAL-VOLUME RESULTS

dHvA frequency measurements at symmetry orientations are shown in Table I and compared with the results of the nonlocal calculation. A local calculation was also made, using the method given in I, to fit the corrected and more accurate dHvA frequencies. In this case the parameters were the form factors, V_{111} and V_{200}, the Fermi energy, and a spin-orbit parameter λ. As one can see, the rms fractional deviation is somewhat smaller for the nonlocal model, but for both models the differences between experiment and calculation, excluding orbit ξ, are less than 2%. (Orbit ξ has been omitted from these estimates because of the larger discrepancies. We do not know why the agreement is not better for this orbit.) In Table II the parameters used in both fits are given. In the same table are shown the form factors evaluated at the symmetry point W for the nonlocal model and the square-well depths which correspond to the form factors used in the local model. In the case of the nonlocal model, these form factors are only representative since there is considerable variation as mentioned earlier (Table III). The spin-orbit parameters are larger than the atomic value; for the nonlocal case $\lambda_1 \approx 1.6\lambda_{so}^a$, where λ_{so}^a is the value of λ_1 [Eq. (4)] determined from the Pb^{+4} spectra, while in the local case $\lambda \approx 1.3\xi_p$, where ξ_p is the atomic spin-orbit-coupling parameter obtained from the lead atom.

In order to maintain compensation, it was necessary to calculate both the third-zone-electron volume V_e and second-zone-hole volume V_h and keep them equal. From the derivatives with respect to energy, dV_e/dE and dV_h/dE, the electron and hole densities of states were determined (Fig. 3). The total density of states $\mathfrak{N}_T(E)$ is given by the sum of the magnitudes of the electron and hole densities of states, and we find $\mathfrak{N}_T(E) \approx 7.4$ Ry^{-1} $atom^{-1}$ which is in agreement with I. (The ratio of the measured to calculated densities of states is about 2.3.) Also, according to our model the slope of the density of states at the Fermi surface is negative $[d\ln\mathfrak{N}_T(E)/d\ln E \approx -1.8]$. However, there

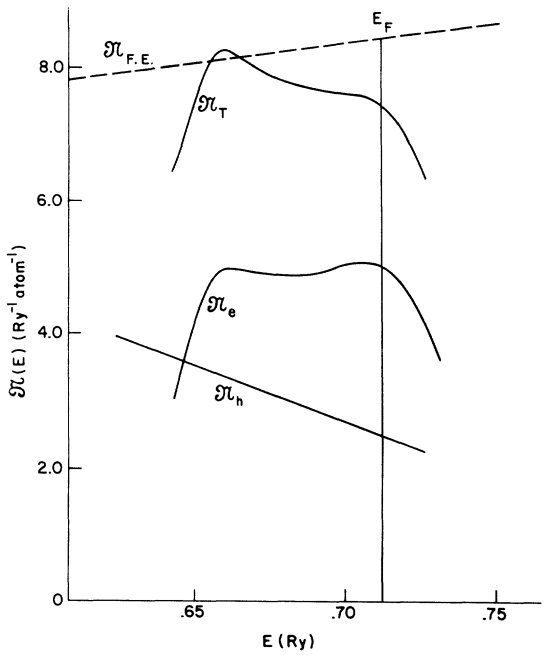

FIG. 3. Density of states in the neighborhood of E_F as calculated from the nonlocal model. The contributions from the second and third bands, $\mathfrak{N}_h$ and $\mathfrak{N}_e$, respectively, are shown. The free-electron model is shown by a dashed curve. The contribution from the fourth band has not been calculated but begins about 0.009 Ry above E_F. The spin degeneracy has been included.

may be large errors in this result, as two numerical derivatives of the electron and hole volumes are required.

We have assumed that the fourth zone is empty in these estimates, which is true for our nonlocal model but not for the local model. We have no experimental evidence for fourth-zone electrons, but the pieces might be very small and missed in our field-modulation experiments. Tobin *et al.*[29] have data which might be explained by the existence of small electron pockets in the fourth zone, but the data are also amenable to other interpretations such as mixing frequencies. Therefore, one of the constraints we have placed on our model is that the fourth zone is empty. (With the local model we were not able to maintain an empty fourth zone and obtain a good fit to the dHvA measurements.)

There have been a number of experiments on dilute alloys of lead which yield information about the density of states and its slope at the Fermi surface. From measurements of superconducting critical fields in lead with Tl as an impurity, Sekula and Kernohan[30] found that, assuming a rigid-band model, there was a peak in the density of states at about 0.14 eV below the pure-lead Fermi energy which might correspond to the weak maximum in

TABLE IV. Lowest-energy eigenvalues at symmetry points (Ry).[a]

Point	Local	Nonlocal	Local	Nonlocal	Local	Nonlocal	Local	Nonlocal
Γ	−0.0172	−0.0074	1.3022		1.4437		1.8813	
ω	0.3322	0.4167	0.5902	0.5062	0.6756	0.6610	0.7069	0.7210
χ	0.3365	0.3986	0.5126	0.4594	0.9266		0.9912	
K, U	0.3237	0.3950	0.5449	0.4930	0.6470	0.6325	1.0200	
L	0.2244	0.2776	0.4375	0.3908	1.1934		1.3717	
E_F	0.724	0.712						

[a]Nonlocal calculations for energies less than 1.9 Ry only.

our density of states curve about 0.1 eV below the Fermi level. On the other hand, Pech[31] and Chol[32] have made similar measurements and found that the density of states was increasing for energies greater than the pure-lead Fermi energy E_F, but unfortunately there were quantitative differences between the results of the two investigators. Careful measurements of the heat capacity in dilute alloys of Pb with Tl and Bi have been made by Clune and Green.[33] Their experiments suggest that the rigid-band model is valid and that the density of states is decreasing above E_F. Our value for $d\ln\mathfrak{N}_T(E)/d\ln E$ is consistent with their results.

The contribution to the density of states from the fourth band has not been included here, but from the energy differences between the fourth band and the Fermi level at W (Table IV) we estimate, assuming a rigid-band model,[19] that there should be an increase in the density of states at about 7 at.% Bi. Unfortunately, de Haas–van Alphen oscillations probably cannot be observed at such high impurity concentrations in lead, but some alloy studies are in progress here to study the density of states near E_F.

We have also determined $E(k)$ curves for our nonlocal model, but they are rather similar to those in I and are not shown in detail. However, in Table IV we show the energies at symmetry points. The most interesting region is probably near W where we have an energy difference of about 0.8 eV between the level just above the Fermi energy (fourth band) and the next lower energy. This separation probably corresponds to the structure at about 1 eV observed by Liljenvall *et al.*[8] in their optical studies of clean lead films. On the other hand, the separation at W between the fourth and second bands is about 2.8 eV, and this does not agree so well with the structure at higher energies observed by Liljenvall *et al.* At W we find the largest separation between the second and third bands, while Loucks[34] has the greatest separation between bands 1 and 2; although he finds the over-all width between bands 1 and 4 is roughly the same as ours. Since our bands were determined only from a fit at the Fermi energy, we might expect errors in the positions of the lower bands.

For completeness we have also calculated the cyclotron masses and curvatures for some of the extremal orbits and these are presented in Table V. The results are approximately the same as those presented in I. We only wish to point out that the mass-enhancement factor is smaller for the more free-electron-like hole orbits than for the third-zone-electron orbits.

VII. PRESSURE MEASUREMENTS

From model calculations such as we have discussed in the above section it is difficult to ascertain uniqueness. However, pressure measurements have proved useful in the testing of various model descriptions.[35] In Table I experimental pressure derivatives of dHvA frequencies are compared with the predictions of both nonlocal and local models. The local-model results have been obtained from a calculation of the form factor curves at several lattice spacings following the approach described by O'Sullivan *et al.*[36] In Fig. 4 these form factors are shown at normal pressure and at a reduced lattice spacing corresponding to 50 kbar. The spin-orbit parameter λ has been assumed to vary with

TABLE V. Cyclotron masses and curvature factors.

Orbit	Direction	Experimental[a]	m^*/m_0 empty lattice	nonlocal	$\frac{m^*_{\text{expt}}}{m^*_{nl}}$[b]	$\frac{\partial^2 A}{\partial k_z^2}$[c]
ν	[100]	1.22	0.630	0.56	2.18	−0.7
ξ	[110]	0.56	0.206	0.22	2.53	2
ξ	[111]	0.68	0.242	0.28	2.42	
ω	[110]	1.26 or 1.41[d]	0.708	0.59		
θ	[111]	1.19	0.583	0.58	2.05	−18
ξ	[001]	0.89	0.189	0.33	2.69	5.2
ψ	[110]	1.10	0.583	0.56	1.97	−8
ψ	[111]	1.12	0.613	0.55	2.04	
ψ	[010]	1.51	0.94[d]	0.75	2.02	

[a]Reference 18.

[b]Ratio of dHvA mass to nonlocal calculated mass.

[c]These curvature factors may be in error by as much as 50% because of small errors made in computing areas.

[d]Reference 5.

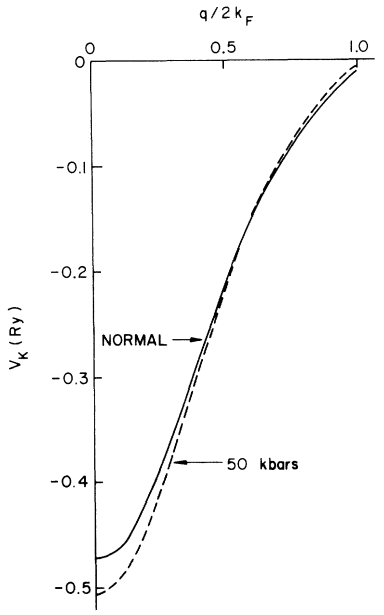

FIG. 4. Model-potential form factors at the normal lattice spacing and the reduced spacing corresponding to 50 kbar.

pressure according to the compressibility, $d\ln\lambda/dP = K_T$.[11] The square-well depths have been assumed to be independent of lattice spacings, but two approaches were used in treating the model-potential radius R_M. For the R_M-constant columns in Table I, the radius was assumed to be independent of lattice spacing. As a second approach, R_M scaled, the radius was assumed to be proportional to the lattice constant. We have no physical justification for the use of the R_M-scaled model.

We see that the local model does not produce a satsifactory prediction of the pressure derivatives. This is especially apparent when we remember that each calculated pressure derivative contains as one term the compressibility scaling factor of $\frac{2}{3}K_T$ ($=1.37\times10^{-3}$ kbar^{-1}) which, in fact, is almost the entire contribution to the changes in the hole surface with pressure given by this model.

The nonlocal R_M-scaled model gives reasonable agreement with experiment, even for the hole surface and accounts very well for the pressure dependence of the ξ orbit. In general, the experimental cross sections increase at about twice the compressibility scaling prediction. This rather large effect seems more plausible when one notes from Fig. 4 that the form factors V_{111} and V_{200} are both negative and decreases in absolute magnitude with pressure tending to make the areas larger. Two exceptions are the ξ_{100} and θ_{111} orbits which change very little. This is because the arm cross sections corresponding to, for example, ζ_{110} are increasing in area with pressure thus tending to reduce the ξ and θ areas; these reductions are at least partially compensated by the increase in area due to compressibility scaling.

VIII. CONCLUSIONS

In summary we have compared our experimental dHvA measurements at normal and high pressure with both nonlocal and local models based upon the Heine-Abarenkov approach.

Either model can be adjusted to provide a fit to the dHvA cross-sectional areas for Pb at normal volume. The local model proved incapable of even qualitatively describing the pressure behavior of the ζ orbit, in particular. In general, the results of our pressure dHvA studies in Pb strongly favor the nonlocal over the local model. We conclude that, in the context of a model potential description for Pb, the effective potential for states near the Fermi energy has a significant wave-number-dependent character. The agreement between the nonlocal-model characterization and the pressure results is particularly good for the R_M-scaled model. However, there is no *a priori* justification for this model. The R_M-constant model underestimates the response of the core electrons to lattice parameter changes with pressure, while the R_M-scaled model overestimates the core response. In the absence of justification for allowing the well diameter to scale with compressibility, we conclude that the close correspondence between the scaled model results and experiment is fortuitous.

The essential results of this work are consistent with conclusions reached in earlier dHvA studies of the effect of hydrostatic pressure on the noble metals.[35,37] Namely, that pressure measurements are a very sensitive technique for revealing the presence of inadequacies in theoretical models of metal band structures which describe the energy bands on constant-energy surfaces. The sensitivity of pressure studies in this respect probably arises from the derivative behavior they induce. Thus, a combination of normal-volume and pressure-dependent dHvA data includes information related to the position of the bands in the Brillouin zone at the Fermi energy and the behavior of the bands for small shifts in the Fermi energy.

In this work, as well as in our earlier studies, we have investigated the dHvA effect in metals, at normal volume and as a function of pressure for limited sets of selected orbits which arise with the magnetic field along crystal symmetry directions. The possibility cannot be discounted, that a more complete normal-volume dHvA study, entailing measurement of dHvA frequencies for fields along nonsymmetry directions, might have allowed us to discriminate between the local and nonlocal models for Pb.

ACKNOWLEDGMENTS

The authors wish to thank Dr. D. R. Stone for assistance with the computations. The support of the University of Maryland Computer Science Center is gratefully acknowledged.

---

*Work supported in part by the U. S. Atomic Energy Commission and by the Advanced Research Projects Agency.

†Present address: Department of Physics, University of Colorado, Boulder, Colo.

[1]Cf. W. L. McMillan and J. M. Rowell, in *Superconductivity*, edited by R. D. Parks (Dekker, New York, 1969), Vol. 1.

[2]Cf. B. J. C. van der Hoeven and P. H. Keesom, Phys. Rev. 137, A103 (1965).

[3]J. R. Anderson and A. V. Gold, Phys. Rev. 139, A1459 (1965). Hereafter this work will be referred to as I.

[4]R. T. Mina and M. S. Khaikin, Zh. Eksperim. i Teor. Fiz. 45, 1304 (1963) [Sov. Phys. JETP 18, 896 (1964)].

[5]K. Sh. Agababyan, R. T. Mina, and V. S. Pogosyan, Zh. Eksperim. i Teor. Fiz. 54, 721 (1968) [Sov. Phys. JETP 27, 384 (1968)].

[6]J. A. Rayne, Phys. Rev. 129, 652 (1963).

[7]A. I. Golovanashkin and G. P. Motulevich, Zh. Eksperim. i Teor. Fiz. 53, 1526 (1967) [Sov. Phys. JETP 26, 881 (1968)].

[8]H. G. Liljenvall, A. G. Mathewson, and H. P. Myers, Phil. Mag. 22, 243 (1970).

[9]R. Stedman, L. Almquist, G. Nilsson, and G. Raunio, Phys. Rev. 163, 567 (1967).

[10]W. J. O'Sullivan and J. E. Schirber, Cryogenics 7, 118 (1967).

[11]J. R. Anderson, W. J. O'Sullivan, and J. E. Schirber, Phys. Rev. 153, 721 (1967).

[12]D. Shoenberg and P. J. Stiles, Proc. Roy. Soc. (London) 281, 62 (1964).

[13]R. W. Stark and L. R. Windmiller, Cryogenics 8, 272 (1968).

[14]J. E. Schirber, Cryogenics 10, 418 (1970).

[15]I. Templeton, Proc. Roy. Soc. (London) 292A, 413 (1966).

[16]J. E. Schirber and W. J. O'Sullivan, Solid State Commun. 7, 709 (1969); J. Phys. Chem. Solids Suppl. 32, 57 (1971).

[17]A. V. Gold, Phil. Trans. Roy. Soc. (London) A251, 85 (1958).

[18]R. A. Phillips and A. V. Gold, Phys. Rev. 178, 932 (1969).

[19]J. R. Anderson and D. C. Hines, Phys. Rev. B 2, 4752 (1970).

[20]D. L. Waldorf and G. A. Ahlers, J. Appl. Phys. 33, 3266 (1962).

[21]V. Heine and I. Abarenkov, Phil. Mag. 9, 451 (1964).

[22]I. Abarenkov and V. Heine, Phil. Mag. 12, 529 (1965).

[23]A. O. E. Animalu and V. Heine, Phil. Mag. 12, 1249 (1965).

[24]A. O. E. Animalu, Phil. Mag. 13, 53 (1966).

[25]C. E. Moore, *Atomic Energy Levels*, Natl. Bur. Std. (U.S.) Circ. No. 467 (U. S. GPO, Washington, D.C., 1958), Vol. 3.

[26]R. W. Shaw and W. A. Harrison, Phys. Rev. 163, 604 (1967); R. W. Shaw, *ibid.* 174, 769 (1968).

[27]See, for example, S. D. Conte, *Elementary Numerical Analysis* (McGraw-Hill, New York, 1965), p. 169.

[28]This approach is similar to that used by P. Soven, Phys. Rev. 137, A1706 (1965).

[29]P. J. Tobin, D. J. Sellmyer, and B. L. Averbach, Phys. Letters 28A, 723 (1969).

[30]S. T. Sekula and R. H. Kernohan, J. Phys. Chem. Solids 27, 1863 (1966).

[31]M. Pech, J. Phys. Radium 23, 591 (1962).

[32]P. G. Chol, J. Phys. Radium 25, 374 (1964).

[33]L. C. Clune and B. A. Green, Jr., Phys. Rev. B 1, 1459 (1970).

[34]T. L. Loucks, Phys. Rev. Letters 14, 1072 (1965).

[35]J. E. Schirber and W. J. O'Sullivan, Phys. Rev. 184, 628 (1968); Colloq. Intern. Centre Natl. Rech. Sci. (Paris) 188, 113 (1970).

[36]W. J. O'Sullivan, J. E. Schirber, and J. R. Anderson, Solid State Commun. 5, 525 (1967).

[37]W. J. O'Sullivan, J. E. Schirber, and A. C. Switendick, Phys. Rev. B 2, 1443 (1970).